Applicability of the cohesive model to engineering problems: On Parameter identification for ductile materials

Ingo Scheider[1a], Norbert Huber[1], and Karl-Heinz Schwalbe[1]

[1]GKSS Research Centre, Institute for Materials Research, Max-Planck-St. 1, 21502 Geesthacht, Germany

[a]ingo.scheider@gkss.de

Keywords: Cohesive model, parameter identification, neural network, structural integrity assessment, ductile damage.

Abstract. The present investigation discusses several methods for parameter identification of the cohesive model. The constitutive behaviour, called traction-separation law, usually contains two parameters for each fracture mode: the cohesive strength, T_0, and the critical separation, δ_0 (or alternatively the cohesive energy, Γ_0). Three identification methods are presented: First, the parameters are determined by a numerical fitting procedure (an Artificial Neural Network is used in the present paper). Second, the parameters are correlated to fracture mechanics quantities and determined experimentally. Third, the cohesive model is used with the micromechanical background of ductile damage of metals, where the separation of the cohesive model can be correlated to the void growth mechanism. While the latter inevitably leads to triaxiality dependence of the cohesive parameters, the values are usually kept constant in the first two methods. It is discussed, whether the assumption of constant parameters holds for the application range of precracked structures under either plane stress or plane strain state. In addition it is investigated how the method of parameter fitting correlates with the other two more physically based methods.

Introduction

The cohesive model was developed some 30 years ago as a numerical tool for the analysis of fracture problems [1]. Since then, many successful applications to a variety of materials and engineering structures have been performed, see e.g. the comprehensive overviews in [2][3]. Common to all versions of the model is that the constitutive behaviour is described by a traction-separation law, which contains at least two parameters for each fracture mode: the cohesive strength, T_0, and the critical separation, δ_0. The cohesive energy, Γ_0, is often used alternatively to δ_0 due to its mechanical association to fracture mechanics quantities. Differences in the application of the cohesive model exist especially in the shape of the traction-separation law and the way of parameter identification. However, for the practical application of the model to engineering structures it is of crucial importance to provide guidance to the user on how to identify the model parameters in a proper and standardized manner.

In this investigation several different methods for parameter identification are discussed. The underlying intention of the model itself with respect to these methods is completely different. If the cohesive model is used as a phenomenological model with parameters that do not have any physical meaning, their identification can be performed using a fitting procedure [4]. An Artificial Neural Network is used in the present paper for this task [5]. Second, since the cohesive model describes a fracture process, the parameters can also be correlated to fracture mechanics quantities, e.g. the cohesive energy, Γ_0, can be set equal to the J-integral at crack initiation, J_i [6], and the cohesive strength is a fracture stress, which is proposed to be determined from notched tensile bars in [6]. Third, the cohesive model can also be used with a micromechanical background. For example if the ductile damage of metals is investigated, the separation process of the cohesive model can be correlated to the void growth mechanism and its degrading material properties [7][8]. While the

latter inevitably leads to triaxiality dependence of the cohesive parameters, the values are usually kept constant in the first two methods. It will be discussed in the present paper, whether the assumption of constant parameters holds for the application range of precracked structures under either plane stress or plane strain state. In addition it will be investigated how the method of parameter fitting correlates with the other two more physically based methods.

Numerical approaches

Cohesive model. The constitutive behaviour of the cohesive model utilised here is a threefold function $T(\delta)$ for normal separation [6]:

$$T(\delta) = T_0 f(\delta) = T_0 \begin{cases} 2\left(\frac{\delta}{\delta_1}\right) - \left(\frac{\delta}{\delta_1}\right)^2 & \delta < \delta_1 \\ 1 & \delta_1 < \delta < \delta_2 \\ 2\left(\frac{\delta - \delta_2}{\delta_0 - \delta_2}\right)^3 - 3\left(\frac{\delta - \delta_2}{\delta_0 - \delta_2}\right)^2 + 1 & \delta_2 < \delta < \delta_0 \end{cases}. \quad (1)$$

The two additional model parameters, δ_1 and δ_2, are used to vary the shape of the traction-separation law. The authors have implemented interface elements as user defined elements (UEL) into ABAQUS for 2D, shell and 3D models [8][9]. This implementation also accounts for tangential and mixed mode fracture, but throughout this paper, only mode I fracture is investigated. The extension of the model used here incorporates the dependence of the parameters δ_0 and T_0 on triaxiality, $h = \sigma_h / \sigma_{eq}$, which is explained in more detail in [8]

Micromechanical model for ductile damage. The failure mechanism of ductile metals is characterised by void nucleation, growth and coalescence. A simple method to model this damage process is the plastic potential derived by Gurson with its extensions by Tvergaard and Needleman. The potential is given by the well-known equation

$$\Phi = \frac{\sigma_{eq}^2}{R^2\left(\bar{\varepsilon}_M^{pl}\right)} + 2q_1 f^* \cosh\left(\frac{3\sigma_h}{2R\left(\bar{\varepsilon}_M^{pl}\right)} q_2\right) - 1 - q_3 f^{*2} = 0, \quad (2)$$

where R is the flow strength of the material surrounding the void, q_1, q_2 and q_3 are model parameters and f^* is a damage variable, which is a function of the void volume fraction, f:

$$f^* = \begin{cases} f & f \le f_c \\ f_c + \kappa\left(f - f_c\right) & f > f_c \end{cases}. \quad (3)$$

The two parameters κ and f_c are additional model parameters. The evolution of the void volume fraction consists of void growth and void nucleation, both driven by plastic straining:

$$\dot{f} = (1 - f)\,\dot{\varepsilon}_{ij}^{pl}\delta_{ij} + A\dot{\bar{\varepsilon}}_M^{pl}, \quad A = \frac{f_n}{s_n\sqrt{2\pi}} \exp\left[-\frac{1}{2}\left(\frac{\bar{\varepsilon}_M^{pl} - \varepsilon_n}{s_n}\right)^2\right] \quad (4)$$

Together with an initial void volume fraction in the virgin material, f_0, and the three parameters for void nucleation, s_n, ε_n, f_n, the model contains 9 parameters. The equations have been implemented in the finite element system ABAQUS [7] as a user defined material (UMAT).

Determination of triaxiality dependent parameters from GTN unitcell simulation. For the micromechanically based identification of the cohesive parameters, a single axisymmetric element with GTN material as described above is pulled under various constant triaxialities. From these simulations, stress versus displacement curves as shown in Figure 1 can be extracted and serve as traction-separation laws in the following. The maximum value in each curve characterizes the cohesive strength, T_0, which is plotted as black symbols in Figure 2. The values are approximated by an exponential function of the form

$$\frac{T_0}{\sigma_Y} = C_0 - C_1 \exp\left(\frac{h_1 - h}{h_2}\right), \tag{5}$$

see the black line in the figure. In a second step the complete separation curves are approximated by eq. (1) for each triaxiality, which leads to a triaxiality dependent separation energy as shown by the red line in Figure 2.

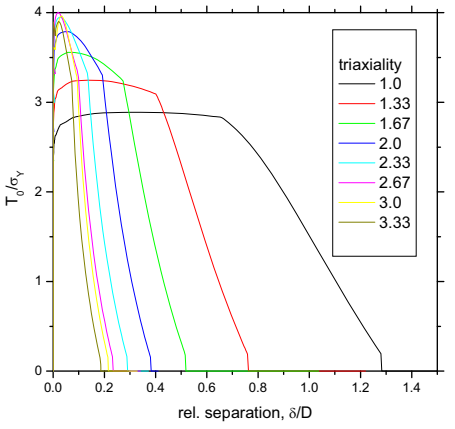

Figure 1: Stress-displacement diagram of an axisymmetric GTN single element simulation under various triaxialities.

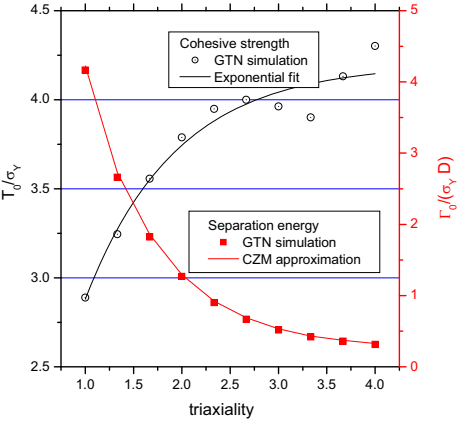

Figure 2: Resulting cohesive strength (black) and separation energy (red) with respect to triaxiality.

Artificial Neural Network: An artificial Neural Network (ANN) can be used for solving complex inverse problems in computational mechanics. The underlying theory is fairly simple: An input vector, X_i, is transformed into the output vector, Y_i, by an interconnected network of neurons assorted in layers as shown in Figure 3. Each single neuron has multiple inputs, y_i, drawn as arrows in the figure, and a single output, v_j, which is a linear combination of these inputs, written as

$$v_j = w_j + \sum w_{ij} y_i$$

with (6)

$$y_j = f(v_j) = \frac{1}{1+e^{-v_j}}$$

The variables w_{ij} are synaptic weights. Connections exist from one layer to the next (called feed forward), and the output of layer i serves as input for layer i+1 after transformation using a smooth sigmoidal function as given also in eq. (6).

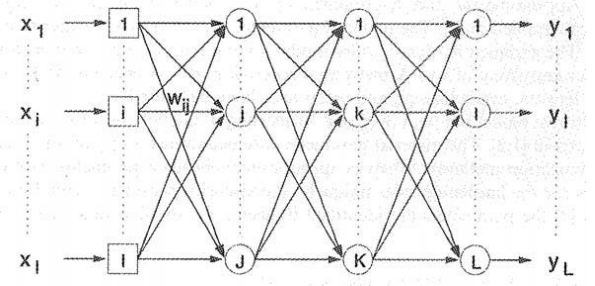

Figure 3: Sketch of a multilayered Artificial Neural Network (from [5])

The ANN is trained by multiple sets of known correlations between input and output vectors in order to identify the parameters w_{ij} and w_j. The internal minimisation strategy behind that identification procedure is called "resilient back-propagation", described in [5]. As a result approximate solutions for unknown output vectors can be calculated.

In the present case the ANN is used to develop a relation between the shape of a curve of experimentally measurable quantities such as force versus elongation, and the cohesive parameters, T_0 and Γ_0. Therefore, the input for the neural network are a small number of sampling points F_i at distinct elongations (the number of sampling points equals the number of input neurons) and the two cohesive parameters are the output neurons, so the number is always 2. The number of layers is chosen to be 3. Training sets are generated by a number of simulations with different cohesive properties and the respective structural response.

After training, the Neural Network is used to determine the cohesive parameters by using the experimental data as the input vector, for which the ANN then calculates the output

Examples

In the following subsections, several tests on fracture specimens are evaluated and simulated using at least two out of the three methods for parameter identification:

1. Parameter identification by fracture mechanics considerations
2. Numerical fitting of the parameters using ANN.
3. Micromechanical considerations

The approaches 1 and 2 can be combined since the fracture mechanics considerations may lead to starting values for the numerical optimization as well.

Fracture specimens made of Aluminium sheet. Various specimen types have been machined of an Al5083 T321 metal sheet (thickness 3 mm), from which the small C(T) and M(T) specimens are discussed here. Detailed studies on these specimens are given in [11],[12]. Since the specimens are thin-walled and break in a slanted fracture mode, plane stress conditions can be assumed. Even

though many specimens have been tested, the crack initiation point cannot be specified accurately, so a range of $J_i = 7\ldots13$ kJ/m² is given. The cohesive strength is proposed to be determined by testing of round notched bars in [6], which is apparently not possible in sheet material. However, the fracture stress of the smooth tensile bar is 485 MPa with failure occurring in a slanted fracture mode, the same in which the fracture specimens failed. The stress value can be used as a lower bound for the cohesive strength, since the maximum local stress at fracture must be higher than this section average value.

In [11] the cohesive model parameters have been determined by trial and error already, leading to $\Gamma_0 = 10$ kJ/m² and $T_0 = 560$ MPa. In this paper, more accurate values will be determined by an ANN training with parameter sets in the neighbourhood of the previously determined values for the C(T) and the M(T) specimen separately. The values used for training of the ANN (black symbols) and the eventually identified optimized values for the various specimens (red symbols) are shown in Figure 4. Even though a single set of constant parameters has been used to simulate all fracture specimens in the previous publications, the difference of the values is not negligible.

As shown in Figure 1 already, a higher triaxiality leads to a higher cohesive strength and a lower separation energy. Thus it can be deduced from the optimized parameters that the triaxiality in the C(T) specimen is higher than in the M(T) specimen, which is confirmed by Figure 5, where the triaxialities ahead of the crack tips of C(T) and M(T) specimens are shown for crack initiation and for $\Delta a = 4$ mm.

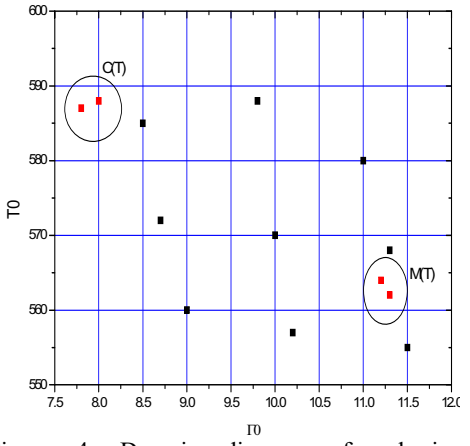

Figure 4: Domain diagram of cohesive parameters, T_0 and Γ_0 for identification. Black symbols are simulations performed for training of the ANN, red symbols are the retrieved parameters for C(T) and M(T) specimen, resp.

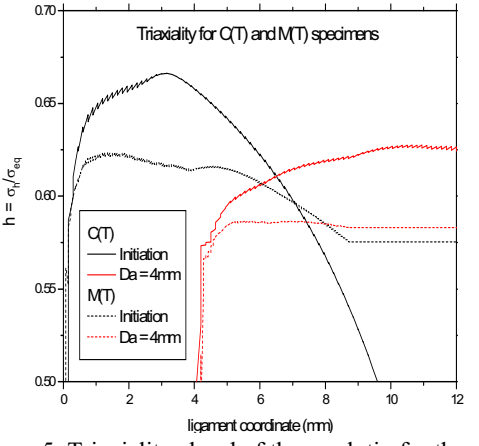

Figure 5: Triaxiality ahead of the crack tip for the C(T) specimen (solid line) and M(T) specimen (dashed line), at initiation (black) and at $\Delta a = 4$ mm.

The results of the simulations with the optimized parameters are shown in Figure 6 for the C(T) and the M(T) specimens. An exceptionally close agreement is achieved with the values shown in Figure 4. However, since only a single fracture specimen should suffice for the determination procedure, it is necessary to know, how large the error is when the M(T) specimen is simulated using the parameters determined with the C(T) specimen and vice versa. These results are also shown in Figure 6. The difference is visible but still in fairly good agreement with the experiment. It must be noted that the R-curve examined from the M(T) simulation using the parameters of the

C(T) specimen is conservative (that is, lower), whereas the one of the C(T) specimen using the M(T) parameters is not.

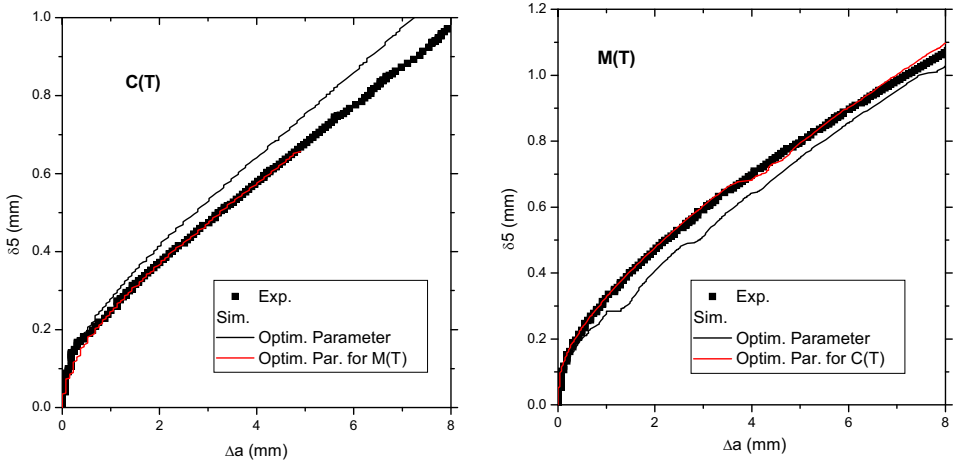

Figure 6: δ_5 R-curves for C(T) specimens (left) and M(T) specimens (right) with parameters optimized for each specimen type. Additionally shown: R-curves using parameters of the respective other specimen.

C(T) specimens made of an RPV steel. A large database containing experimental data from fracture mechanics tests on a ferritic pressure vessel steel has been generated by European research laboratories [10]. In [13], the C(T) specimen was analyzed by a 3D finite element analysis using the cohesive model. As mentioned before J_i might be used for the cohesive energy, Γ_0. The values determined for J_i (actually J at $\Delta a = 0.05 \ldots 0.1$ mm) were 70…150 kJ/m². Notched bars, which are necessary to determine the cohesive strength, T_0, were not available. A parameter study was therefore performed with a starting value of $\Gamma_0 = 70$ kJ/m² and T_0 in the range 1700…2100 MPa (more than 3 times the yield strength, which is a presumable value for this kind of steels). It turned out that the Γ_0 value was too high, and the optimized values shown in Figure 7 were $\Gamma_0 = 35$ kJ/m² and $T_0 = 2100$ MPa. The reason for this discrepancy can be explained, if the J_i/Γ_0 ratio is plotted versus the ratio T_0/σ_Y. As shown in Figure 8, the separation energy equals the J-integral at crack initiation, when the value of T_0 approaches the yield strength, i.e. for rather brittle materials. However, if the value of T_0 is high, the ratio is in general much larger than one. This reveals that the equation $J_i = \Gamma_0$ is too simple and can only be applied to purely elastic materials, but it can be used as an upper bound for Γ_0.

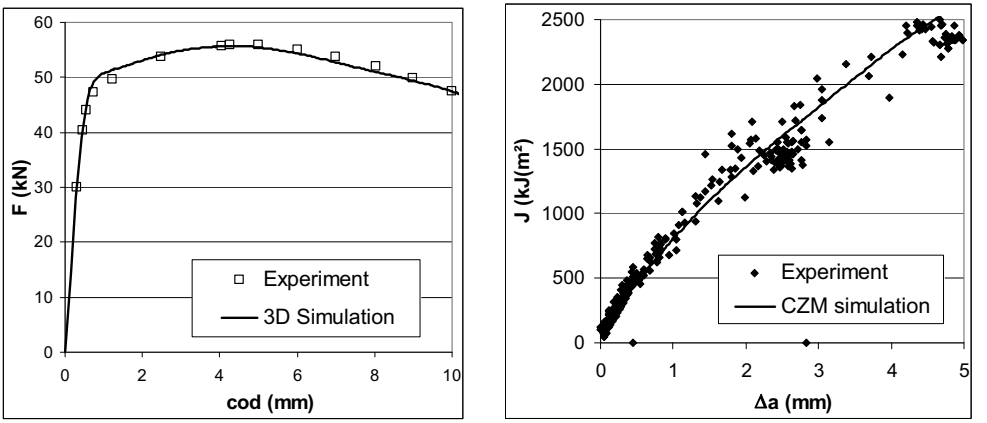

Figure 7: Force vs. COD (left) and J R-curve (right) of RPV steel. Experiment (symbols) and 3D cohesive model simulation.

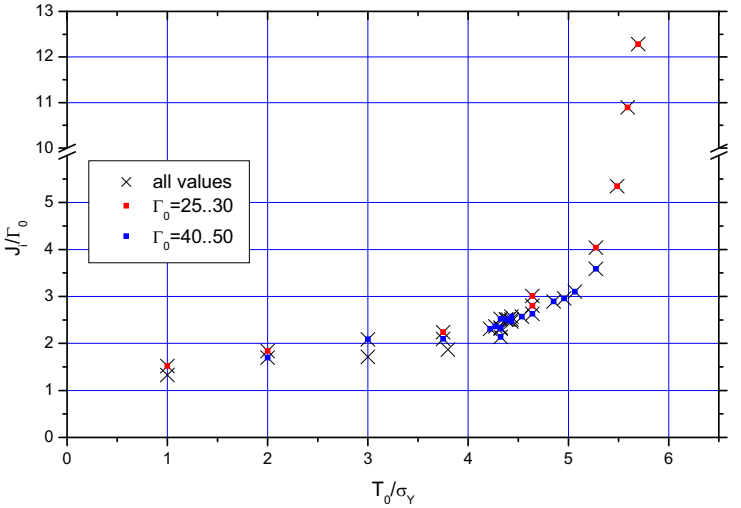

Figure 8: Ratio of J_i/Γ_0 plotted versus the ratio T_0/σ_Y, which shows the influence of plasticity on the crack driving force.

Fracture specimens made of a structural steel. In ref. [8] a study was performed on a ferritic steel designated as FeE 460 using micromechanically based cohesive parameters as described in the previous section. The result of this investigation is shown in Figure 9. From these two figures, which show the *J*-R curves for a C(T) and a M(T) specimen, respectively, several conclusions can be drawn. First, the GTN simulation is in close agreement to the experiment for the C(T) specimen, but not for the M(T) specimen. Second: The cohesive model simulation with triaxiality dependent parameters is somewhat jagged, which results from the strong changes in the triaxiality ahead of the crack tip, which do not occur for the M(T) specimen. However, the curve is a good approximation of the experiment in both cases. If the cohesive parameters are kept constant, a very good agreement with the experiment is achieved for the C(T) specimen, for which the parameters are optimized, and still a rather good (but non-conservative) agreement is reached for the M(T)

specimen. However, it must be noted that the tendency is different from the results for the Al5083 material shown above, where the R curve for the M(T) specimen was conservative with parameters taken from the C(T) specimen. The reason for this discrepancy becomes visible if the parameters are plotted in a domain diagram, see Figure 10. For an unknown reason the optimal separation energy for the C(T) specimen is very high and the cohesive strength is rather low, as commonly seen only at a very low triaxiality. In addition, one can see that the parameter values determined from the M(T) specimen do not coincide with a point on the curve for the triaxiality dependent parameters, but are close to the values for $h \approx 1.7$.

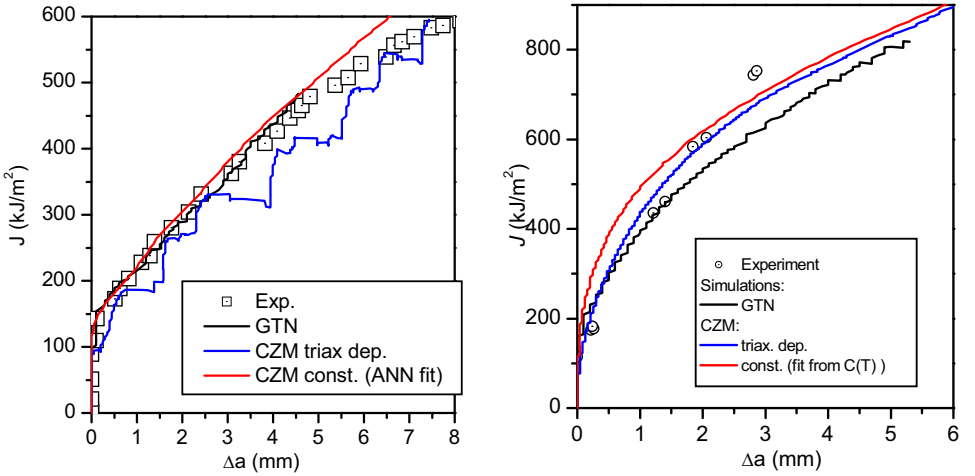

Figure 9: *J* R-curves for C(T) specimen (left) and M(T) specimen (right). Experiments (symbols) are compared to several simulations.

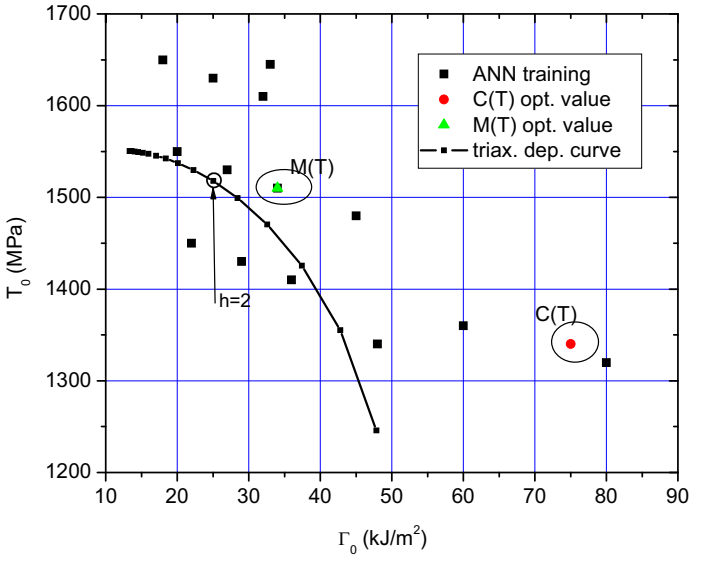

Figure 10: Domain diagram of the cohesive parameters for a ferritic steel. The black dots show the sets used for ANN training, and the curve shows the parameters for the triaxiality dependent model.

Conclusions

Three methods have been presented here to determine the cohesive parameters for crack growth simulation of different materials.

The first method, that is the experimental determination of cohesive parameters, did not always lead to acceptable results. The crack driving force at initiation, J_i, is in general not equal to the separation energy, but contains additional energy dissipated by plasticity. The cohesive strength, T_0, might be determined by round notched bars, but this is difficult if only thin sheets are available. Smooth round bars or flat tensile bars underestimate the cohesive strength if local necking occurs before fracture. However, together with the numerical fitting, fracture mechanics based parameters are useful as a starting point for the optimization. With the combination of these two methods, in all simulations a very close agreement between experiment and simulation could be achieved, and the transferability of the parameters is also fairly good.

The parameter identification using a micromechanical model gives also good results, and the transferability seems to be better than with constant parameters, but at the cost of robustness of the procedure. In addition, a second model has to be used, which is not favourable in engineering applications.

References

[1] A. Hillerborg, M. Modeér and P.E. Petersson, Cement. Concrete Res. 6 (1976), p. 773.

[2] M. Elices, G.V. Guinea, J. Gómez and J. Planas, Eng. Fract. Mech. 69 (2002), p. 137.

[3] W. Brocks, A. Cornec and I. Scheider, in: *Comprehensive Structural Integrity*, Vol 3, edited by Milne et al. (2003), p. 127.

[4] D. Steglich and W. Brocks, in *Comprehensive Structural Integrity*, Vol 11, edited by Milne et al. (2007), p. 107.

[5] N. Huber and C. Tsakmakis: Comput Methods Appl. Mech. Engrg. 191 (2001), p. 353.

[6] A. Cornec, I. Scheider and K.-H. Schwalbe: Eng. Fract. Mech. 70 (2003), p. 1963.

[7] T. Siegmund and W. Brocks: Eng. Fract. Mech. 67 (2000), p. 139.

[8] I. Scheider, submitted to Eng. Fract. Mech. (2008)

[9] I. Scheider and W. Brocks, Comput. Mater. Sci. 37 (2006), p. 101.

[10] J. Heerens and D. Hellmann, Eng. Fract. Mech. 69 (2002), p. 421.

[11] I. Scheider and M. Schödel, Adv. Eng. Mater. 8 (2006), p. 410.

[12] I. Scheider, M. Schödel, W. Brocks and W. Schönfeld, Eng. Fract. Mech. 73 (2006), p. 252

[13] R. Gurunathan, Master thesis University Stuttgart, GKSS internal report GKSS/WMS/08/02 (2008)